Journal of Materials Chemistry C

Accepted Manuscript

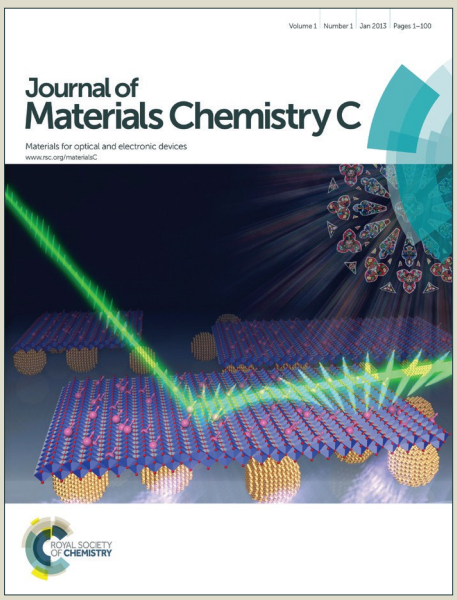

ROYAL SOCIETY OF CHEMISTRY

www.rsc.org/materialsC

CVD Synthesis of carbon spheres using NiFe-LDHs as catalytic precursors. Structural, electrochemical and magnetoresistive properties

Jose A. Carrasco,[a] Helena Prima-Garcia,[a] Jorge Romero,[a] Jesús Hernández-Saz,[b] Sergio I. Molina,[b] Gonzalo Abellán,[a,c,*] and Eugenio Coronado[a,*]

[a] *Instituto de Ciencia Molecular (ICMol), Universidad de Valencia, Catedrático José Beltrán 2, 46980, Paterna, Valencia, Spain.*

[b] *Departamento de Ciencia de los Materiales e Ingeniería Metalúrgica y Química Inorgánica, Universidad de Cádiz, 11510 Puerto Real, Cádiz, Spain.*

[c] *Department of Chemistry and Pharmacy and Institute of Advanced Materials and Processes (ZMP), University Erlangen-Nürnberg, Henkestr. 42, 91054 Erlangen and Dr.-Mack Str. 81, 90762 Fürth, Germany.*

- Corresponding authors
- Tel.: +49 911 65078-65031. Fax: +49 911 65078-65015, *E-mail address*: gonzalo.abellan@fau.de (Gonzalo Abellan)
- Tel.: +34 96 354 4415. Fax: +34 96 354 3273. *E-mail address*: eugenio.coronado@uv.es (Eugenio Coronado)

Abstract

Gram-scale synthesis of carbon spheres with a diameter of *ca.* 740 nm has been achieved by means of a chemical vapour deposition method using NiFe-layered double hydroxides as a solid catalytic precursor. The presence of the catalyst ($FeNi_3$) allows controlling the final size distribution, resulting in a monodisperse sample. Their structural properties exhibited a high degree of graphitization according to their I_D/I_G ratio. In addition, their morphological features were unveiled by FIB-SEM and HRTEM, showing that they are formed by solid inner cores, and presenting labile chain-like structures due to accretion procedures. The solution and posterior sonication of the samples in toluene gave rise to the well-defined isolated spheres. The textural and electrochemical properties of the spheres have been tested showing a non-mesoporous structure with a good behaviour as electrode materials for supercapacitors due to the presence of redox functionalities on their surface. Finally, magneto-transport measurements have been carried out, demonstrating semiconductor behaviour, as well as a positive magnetoresistance effect (*ca.* 72 %) for the lowest studied temperature (2 K).

1. Introduction

Since the discovery of fullerene (C_{60}) by Kroto et al. in 1985,[1] many works have been published around the field of the so-called carbon nanoforms (CNF). These carbon-based materials include a wide variety of sizes and shapes ranging from C_{60} to metallofullerenes, carbon fibers, nanotubes (single-wall, multi-wall…), nano-onions, nanohorns, nanobuds, spheres or graphene, among others.[2] The interest in the different synthetic carbon allotropes relies on their outstanding properties and applications, as recently highlighted by the ubiquitous graphene. Among this family, the spherical carbon structures like C_{60}, or carbon nano-onions have attracted increasing attention in the last years. One of these forms are the carbon spheres (CS), formerly known as carbon blacks.[3] The curved structure of CS is a consequence of the presence of pentagonal and heptagonal rings within the hexagonal framework of carbon, allowing the system to adopt their characteristic morphology.[4]

The carbon spheres can be classified according to different parameters, like their size, nanometric texture or internal structure.[5–8] Recently, Deshmukh *et al.* have reviewed the different techniques employed for the synthesis of CS, pointing out the chemical vapour deposition (CVD) as one of the most versatile synthetic approaches.[9]

These carbonaceous forms show a wide range of potential applications due to their thermal stability, electronic properties, high surface area or low density. Furthermore, their unclosed graphitic flakes give rise to the presence of dangling bonds throughout the spheres surface, increasing their reactivity and boosting their applicability in adsorption, lubricants, tribological coatings, catalysis, batteries, supercapacitors or fuel cells among others.[10–15] Conversely, when it comes to their transport and magnetic properties, the list of examples is very scarce,[16,17] despite their potential as electronically active reinforcing agents of functional composites.[18,19] Indeed, the recent discovery of organic magnetoresistance (OMAR) in graphene and other related nanocarbons has significantly increased the attention paid to these systems, as they are promising materials for flexible, low-cost and transparent electronics.[20–25] Therefore, the cost-effective production of magnetoresistive CS is of great interest in the development of new hybrid composites and functional polymers.

Herein, we have synthesized monodisperse carbon spheres in a gram-scale by means of a CVD procedure using NiFe-layered double hydroxides (LDH) as catalytic precursor.[26] The NiFe-LDH materials have demonstrated their utility as catalysts in the low-temperature synthesis of several carbon nanoforms, including carbon nano-onions,[23] bamboo-like carbon nanotubes or even graphene –when they are used as precursors for the preparation of hybrid $FeNi_3$–graphene nanocomposites. [28–30]

We have thoroughly characterized the as-obtained spheres by means of XRD, Raman, FT-IR, TG, FESEM, FIB-SEM, HRTEM, DLS, N_2 isotherms, XPS and Electrochemistry. Furthermore, their magneto-transport properties revealed a semiconducting behaviour with an intrinsic large MR of *ca*. 72%.

2. Experimental methods

2.1 Chemicals

All chemical reagents $Ni(NO_3)_2 \cdot 6H_2O$ (Aldrich); $Fe(NO_3)_3 \cdot 9H_2O$ (Sigma-Aldrich); triethanolamine (TEA), $C_6H_{15}NO_3$ (Sigma-Aldrich); Urea, $CO(NH_2)_2$ (Fluka) and Ethanol Absolute (Panreac, 99.9%) were used as received without further purification. Ultrapure water was obtained from a Millipore Milli-Q equipment. N_2, H_2/Ar (10%) and ethylene (C_2H_4) were purchased from Linde Material Handling.

2.2. Synthesis of NiFe-CO_3 LDHs

NiFe-CO_3 LDH were synthesized following a modified homogeneous precipitation method by using urea and TEA as ammonium releasing reagent (ARR) and chelating agent, respectively.[27]

In a typical synthesis, the nitrate salts of the metals were dissolved in 50 mL of deionized pure water together with TEA, in order to reach a total metal cation concentration of 20 mM in the final solution, with a ratio Ni:Fe of 3:1 (x = 0.25, being x = $[Fe^{3+}]/([Fe^{3+}] + [Ni^{2+}])$, and a concentration of TEA equimolar with the iron concentration (5 mM). Next, 50 mL of an aqueous solution of urea (35 mM) were added. The excess of urea was fixed to be 1.75 times the total metal concentration. The resulting dark brown mixture was placed in a 125 cm^3 stainless steel Teflon-lined autoclave and heated up to 150 ^oC in a previously heated oven. After 48 h, the autoclave was left to cool down at room temperature and the final yellowish fine powder was filtered and dried in a vacuum. The pH value of the remaining solution was found to be around 8.

2.3. Synthesis of Carbon spheres

Carbon spheres were synthesized by means of a chemical vapour deposition process (CVD). In a typical procedure, 25 mg NiFe-LDH were placed at the centre of a horizontal quartz tube, which was inserted into a tubular furnace at atmospheric pressure. The furnace was heated under flowing N_2 (100 mL min^{-1}) up to 900 ^oC in a 5 ^oC min^{-1} scan rate. When the temperature was reached, a reduction treatment with H_2 (50 mL min-1, mixture of H_2 10% in Ar) was performed during 5 min before switching the gas for the carbon source, ethylene (C_2H_4, 100 mL min^{-1}), during 60 more min at 900 ^oC. Then, the furnace was cooled to room temperature under N_2 protection, and the sample was collected from the quartz tube. Control experiments in absence of the NiFe-LDH were also carried out keeping the same experimental conditions.

2.4. Thermal Treatment

The *as*-synthesized carbon spheres were annealed at 800 ^oC in order to eliminate organic impurities. In a typical procedure, the sample was placed in a holder at the centre of a horizontal quartz tube inserted into a furnace at atmospheric pressure. The furnace was heated up to 800 ^oC under N_2 atmosphere (100 mL min^{-1}) in a 2 ^oC min^{-1} scan rate. When the temperature was reached, the system was cooled to room

temperature under N_2 protection. Finally, the annealed spheres were collected from the holder.

2.5. Physical Characterization

X-ray powder diffraction (XRPD) patterns were obtained using a PANalytical Empyrean X-ray powder diffractometer using the copper radiation (Cu-Kα = 1.54178 Å). Samples were mounted on a flat sample plate. Profiles were collected in the $2.5^o < 2\theta < 90^o$ range with a step size of 0.05^o. The Raman measurements (Jobin-Yvon LabRam HR 800 Raman Microscope) were carried out at room temperature with the 532 nm line of an Ar ion laser as an excitation source. Spheres morphology was studied by means of field emission scanning electron microscopy (FESEM) performed on a Hitachi S-4800 microscope operating at an accelerating voltage of 20 kV over metallized samples with a mixture of gold and palladium for 30 s. FEI dual-beam FIB-SEM Quanta 200 3D equipment operating at 30 kV was used to mill the spheres and observe their inner structure and prepare a lamellae by *in situ* lift-out method.[32] High-resolution transmission electron microscopy (HRTEM) studies were carried out on Tecnai G2 F20 and Jeol 2100 microscopes operating at 200 kV. Samples were prepared by dipping a sonicated suspension of the sample in toluene on a carbon-coated copper grid. Metallic atomic composition of bulk samples was determined by means of electron probe microanalysis (EPMA) performed in a Philips SEM-XL30 equipped with an EDAX microprobe. Carbon, nitrogen and hydrogen contents were determined by microanalytical procedures by using a LECO CHNS. Infrared spectra were recorded in a FT-IR Nicolet 5700 spectrometer in the 4000–400 cm^{-1} range using powdered samples diluted in KBr pellets. Thermogravimetric analysis of the compounds were carried out with a Mettler Toledo TGA/SDTA 851 apparatus in the 25 – 800 ^oC temperature range under 10 $^oC \cdot min^{-1}$ scan rate and an air flow of 30 $mL \cdot min^{-1}$. The porous texture was characterized by N_2 adsorption at 77 K in an AUTOSORB-6 apparatus. The samples were previously degassed for 4 h at 523 K and $5 \cdot 10^{-5}$ bar. Dynamic light scattering (DLS) measurements were recorded at 25 ^oC with a Zetasizer Nano ZS instrument (Malvern Instrument Ltd.) on a freshly prepared sample (1 mg of CS in 10 mL of toluene and sonicated for 30 min). The electrical conductivity and the magneto-resistance measurements were carried out by using a standard four-probe contacts method with Pt wire in a physical property measurement system (PPMS-9) by Quantum Design. The resistivity data were taken from 300 to 2 K and from 0 to 8 T, with

Keithley 2450 as a current source and a Keitley 6514 as an electrometer. The measurements were performed in a pressed pellet of the **CS** with a size of $2.4 \cdot 10^{-4}$ cm^{-2}.

2.6 Electrochemical measurements

The electrochemical analyses were performed using an Autolab electrochemical workstation (PGSTAT-100 potentiostat/galvanostat) connected to a personal computer that uses GPES electrochemical software.

The materials were mixed with acetylene black and PVDF at a mass ratio of 80:10:10 in ethanol and deposited on a nickel foam electrode. The as-prepared nickel foam electrodes were dried overnight at 70 °C and pressed. Each working electrode contained about 1 mg of an electroactive material and had a geometric surface area of about 1 cm^2. A typical three-electrode experimental cell equipped with a stainless steel plate having 4 cm^2 of surface area as the counter electrode and a Metrohm Ag/AgCl (3 M KCl) as the reference electrode were used for the electrochemical characterization of the nanocomposite materials trapped by the working electrodes.

The electrochemical measurements were carried out in aqueous 6M KOH solutions as the electrolyte. Ultrapure water was obtained from Milli-Q equipment. The specific capacitance (C), was calculated from the cyclic chronopotentiometric curves according to eqn (1):

$$C = I\Delta t/m\Delta V \quad (1)$$

where I is the charge/discharge current, Δt is the time for a full charge or discharge, m is the mass in grams of the active material in the electrode layer, and ΔV is the voltage change after a full charge or discharge.

Electrochemical impedance spectroscopy measurements were carried out by applying AC amplitude of 10 mV in the frequency range of 0.01–10^6 Hz at open circuit potential with the help of an impedance spectrum analyser (GAMRY interface 1000 potentiostat). The electrochemical cell was placed in a faradaic cage. Data was analysed with the help of Gamry Echem Analyst v. 6.03 software.

3. Results and discussion

The synthesis of the carbon spheres was achieved by means of a catalytic CVD process at 900 ºC using NiFe–LDHs as catalytic precursor and ethylene as a carbon source during a period of 60 min. After the CVD process, a black solid with metallic brilliance was formed thorough the quartz tube. The sample was collected from the inner part of the quartz reactor, powdered and submitted to a subsequent annealing process at 800 ºC under inert atmosphere in order to eliminate possible organic impurities. The final product was a black powder light in weight; hereinafter named as **CS**. Further characterization of the pristine spheres is depicted in the supporting information (See SI 1).

As recently reported by our group, NiFe-LDHs are excellent catalyst for the synthesis of carbon nanoforms.[26,28] Moreover, we have demonstrated that the calcinated NiFe-LDH preserves the structural integrity, being the in-situ formed $FeNi_3$ nanoparticles the main catalytic seeds.[27] Herein, control experiments consisting on the calcination of NiFe-LDHs at 900 ^{o}C, supplying H_2 but in absence of a carbon source, gave rise to a mixture of $NiFe_2O_4$, NiO and $FeNi_3$ phases as revealed by XRPD (see SI 2.1). However, further experiment with neither H_2 nor ethylene depicted the presence of only a mixture of $NiFe_2O_4$ and NiO, concluding that $FeNi_3$ alloy is the active catalytic species in the CVD reaction, responsible of the growth of carbon nanoforms. Indeed, a low-temperature CVD process at 550ºC with bulk samples leads to a mixture of carbon nanoforms formed by few-layers graphene, carbon fibers and multi-wall carbon nanotubes (see ref. [28] for further information). According to Li and co-workers, these graphitic structures could evolve towards the formation of carbon spheres for larger times of feeding.[33] Herein, the presence of the catalyst is reflected in a decrease in the starting synthesis temperature towards *ca*. 800 ºC, allowing the gram-scale formation of monodisperse **CS** (*vide infra*). On the contrary, carbon sphere control experiments without the presence of catalyst leads to an increase in the temperature to 900 ºC yielding less amount of **CS** with a wide range of dimensions and morphologies, highlighting the crucial role of the NiFe-LDH (Fig. SI 2.2). [34]

Inagaki *et al*.[6,7] reported that the most probable mechanism for the formation of the carbon spheres consists on the dissociation of ethylene (carbon source) at 900ºC into C and H. After that C starts to polymerize forming the so-called basic structural units (BSUs), whilst methane and hydrogen are also formed. Usually, the arrangement of these BSUs leads to three different textures in these carbon forms: concentric, radial and

random.[7] The final disposition of these units depends on the precursor, heating treatment, feeding time and the interface between the carbons and their surroundings during the thermal process.[7,28,29] Anyway, the exact role of the catalyst in the formation of spheres mediated by CVD procedures is not yet fully revealed. It seems that the $FeNi_3$ catalyst may act as a template, providing the nucleation sites for the subsequent sphere formation. Another possibility is its role in the modification and deposition of carbon radicals which are formed in the gas phase, *i.e.,* helping the decomposition of the carbon source instead the polymerization reaction.[9]

XRPD spectrum in **CS** was measured in order to study the graphitic structure of the sample. Fig. 1 A exhibits the presence of a main peak centred at *ca.* 25^{o} and a secondary peak at *ca.* 43.8^{o}, related with the (*002*) and the (*100*) planes of graphite, respectively. The common broadness of the peaks in the carbon sphere spectra indicates a low range in the structural order.[10,28] According to Bragg´s equation, the interlayer spacing d_{002} of our **CS** is 0.3562 nm, which agrees with the literature, [30,31] with a low deviation for the ideal d_{002} space (0.343 nm) in a graphitic structure (JCPDS-ICDD Card No. 41-1487). This value is intermediate between those measured for a carbon fiber (d_{002} = 0.342) and activated carbons (d_{002} = 0.363), which is indicative of a relatively well organised carbon structure.[5]

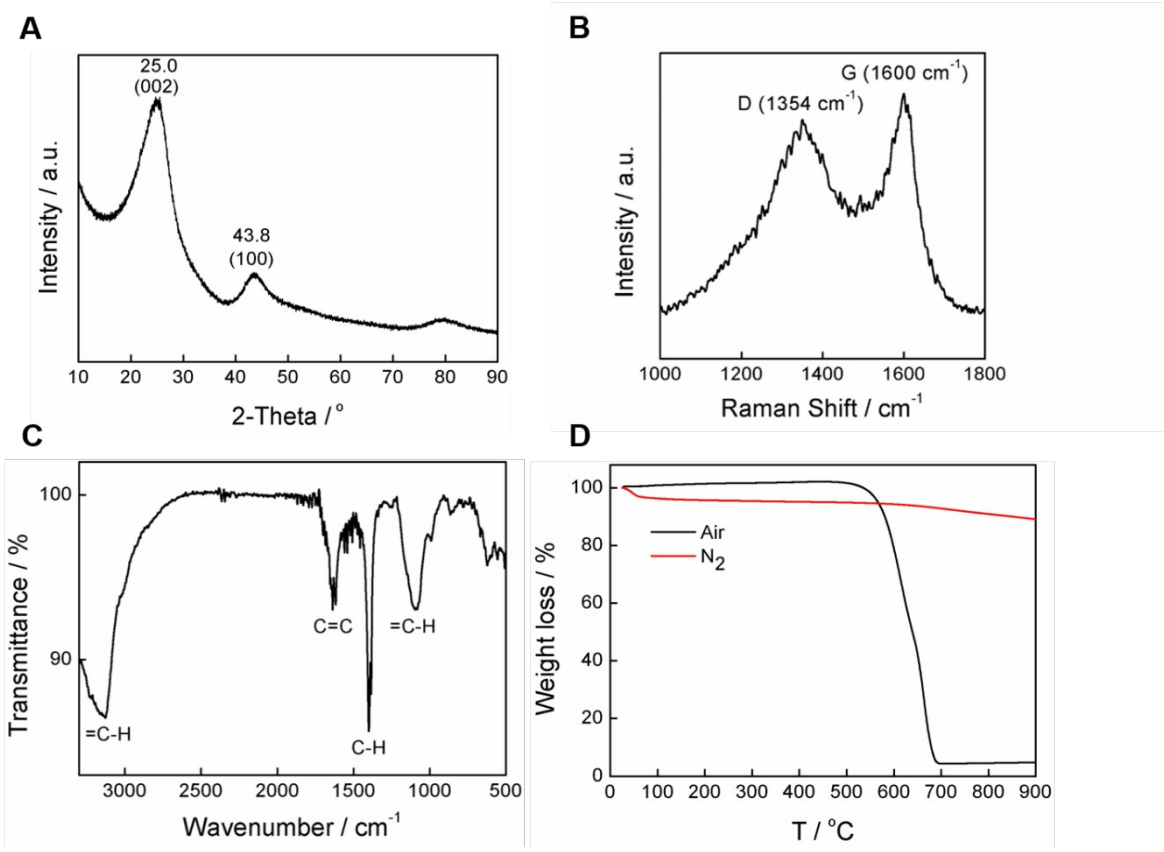

Figure 1. (A) XRPD, (B) Raman and (C) FT-IR spectra of **CS**. (D) TGA of **CS** under air (black line) and nitrogen atmosphere (red).

Raman spectra have been recorded to disclose the graphitic ordering of the **CS**. Fig. 1 B shows a representative Raman spectrum with the characteristic D and G bands centred at 1354 cm^{-1}, and 1590 cm^{-1}, respectively. The D band is related with the defects and the disorder-induced modes, and the G band is associated to the in-plane E_{2g} zone-centre mode, *i.e.* the vibration of sp^2-bonded carbon atoms in a two-dimensional hexagonal lattice. The I_D/I_G ratio is related with the graphitic ordering in carbon materials, high I_D/I_G ratio involves a low degree of graphitization (order) in the carbon system, and *vice versa*. In our sample we measured a I_D/I_G ratio of *ca.* 0.80, showing a higher degree of graphitization (lower I_D/I_G) than most of the other CVD carbon spheres reported to date.[10,33,37,38] Lower I_D/I_G ratios can be achieved in presence of MnO_2 or Ni doping.[39,40] In any case, our results are in accordance with the graphitization trend reported by Nieto-Marquez et al.: Graphite > Carbon nanotubes/nanofibers > Carbon nanospheres > Activated carbon.[10] A further comparison for all the synthesized spheres in the work can be found in SI 3.

FT-IR (Fig 1 C) confirmed the presence of C=C (1637cm^{-1}) and =C-H groups (3100 and 1080 cm^{-1}, stretching and bending modes, respectively) in the **CS**, supporting the presence of a sp^2 structure. Among these, another band at *ca.* 1400 cm^{-1} can be found, related with C-H bending mode.[34]

Furthermore, thermogravimetric analysis (TGA) and differential thermal analysis (DTA) experiments in air and N_2 atmosphere up to 900 ^{o}C were carried out. The thermogravimetric profile reveals that **CS** are stable in air below 530 ^{o}C; at *ca.* 560 ^{o}C they exhibit an abrupt mass loss of *ca.* 95% which ended at 700 ^{o}C (Fig 1 D). According to Serp *et al*. classification of carbon nanoforms based on the maximum of gasification rate,[5] our sample is located in the range of the carbon nano-spheres with a combustion temperature of *ca.* 630 ^{o}C depicted in the DTA (See SI 4). In turn, the experiment under N_2 exhibits a stable thermal behaviour, showing only a weight loss of *ca.* 10% when 900 ^{o}C is reached. It is worth noting that, in presence of air, a slight increase of mass (*ca.* 105%) is observed just before the thermal decomposition; this is attributed to the oxidizing process of the graphitic flakes into oxidized graphite. In contrast, this effect is not seen under N_2.[34,41]

After studying the structural properties of the spheres, their morphology was unveiled by means of FESEM and HRTEM, depicting the spherically characteristic shape of **CS**, with a large quantity of them usually forming aggregates (Fig 2). Accretion of the spheres into clusters of several microns (See SI 5) were described by Kroto *et al.* for feeding times higher than 10 min.[34], or by Pole and co-workers as the result of cooling the system from high- to room temperature.[35] Anyway, it is worth noting that this coalescence is related to the presence of reactive dangling bonds on the surface, which gives them a high surface reactivity.[4,10] Indeed, EDAX analysis of the sample revealed a carbon content of 93.2 atomic % and an oxygen content of 6.8 %. These results are corroborated by C, H, N elemental analysis, with a carbon content of. 93.3% (atomic ratio) and 0.4% of H. No N was detected. Atomic percentages were also corroborated by XPS (See SI 6.1). Furthermore, XPS spectrum of the C_{1s} clearly exhibit a main peak which can be deconvoluted into sp^2 and sp^3 components. No trace of the catalyst (Ni and Fe) was found in the spectra of the **CS** (SI 6.2). Finally, the synthesis of carbon spheres at a higher temperature (1000 ^{o}C) depicted a decrease of *ca*. 1% in the O atomic

percentage (a decrease of *ca*. 11% of the total oxygen content). N signal remains residual (SI 6.1).

The particle size distribution was determined by measuring 50 spheres in the SEM images, giving rise to an average diameter of 740 ± 42 nm. This is in sharp contrast with the wide range of diameters obtained in the control experiments (See SI 2), and highlights the role exerted by the NiFe-LDH catalytic precursor in controlling the size distribution of the spheres.

In order to determine directly whether the spheres are hollow or not, we have taken advantage of a dual beam focused ion beam-SEM instrument. A precise milling was carried out over several spheres. An example of a typical zone where the focused ion milling process has been applied is shown in Figure 2 C. The cross-section acquired after the milling process supplies detailed information of the specimen subsurface, highlighting the existence of a solid inner structure in the spheres, as it is depicted in Fig. 2 D and E.

Furthermore, a lamella thinned down to electron-transparency has been studied by TEM showing the absence of mesopores and the porosity between the carbon spheres (*vide infra*) (Fig 2 F). The preparation of these lamellae is detailed in SI 7.

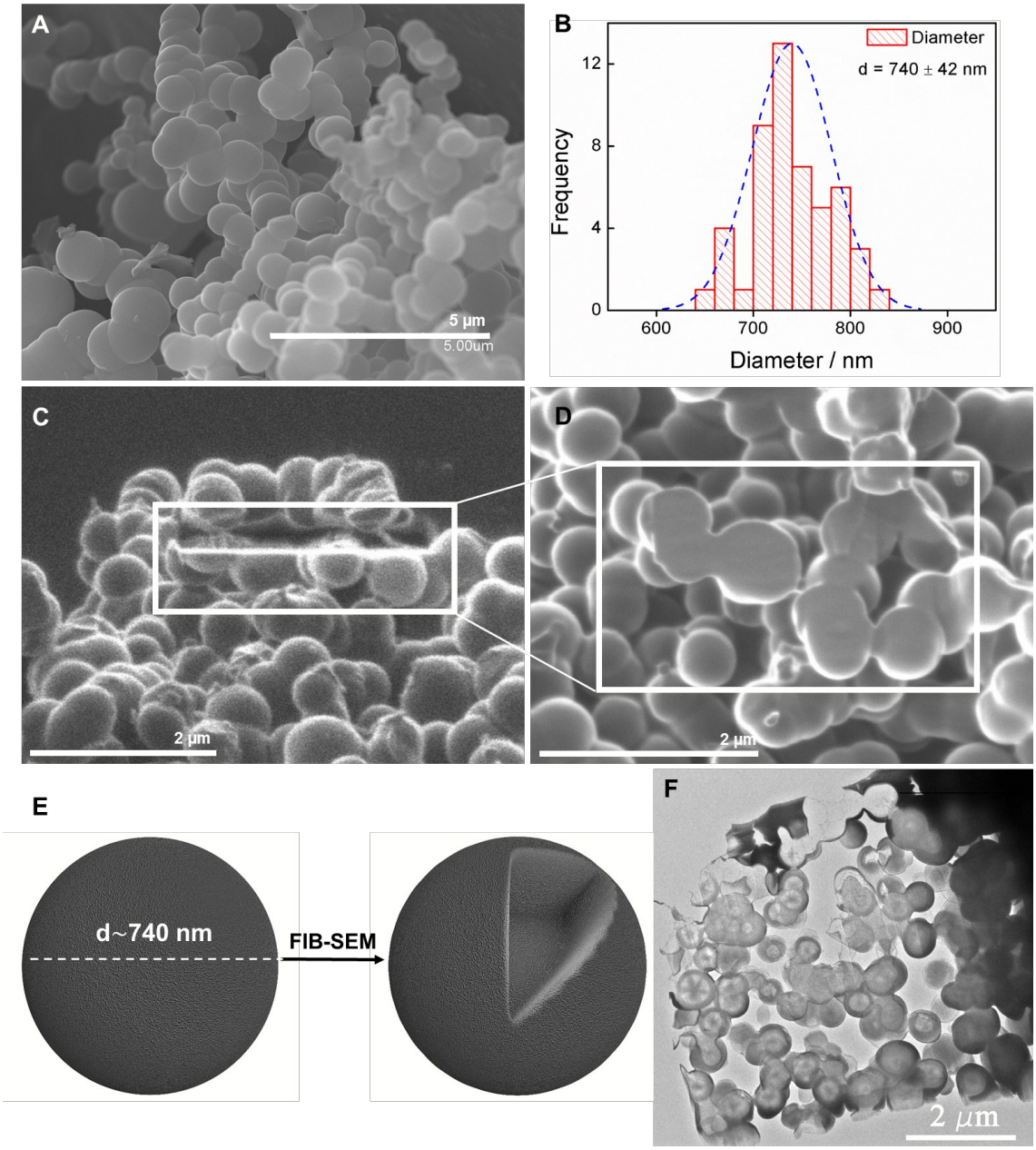

Figure 2. (A) FESEM image of **CS**. (B) Histogram displaying the average diameter taken from FESEM images. (C) FIB-SEM image of the milled region, it is remarked within the white square. (D) FIB-SEM cross-section image of the same region of (C) depicting a solid inner structure. (E) Idealized 3D representation of a sphere before and after the FIB, highlighting the solid inner structure. (F) Bright field TEM image of electron-transparent lamella prepared by FIB-SEM. The porosity between the carbon spheres is highlighted.

HRTEM images displayed nearly perfect spherical morphologies with an average diameter of *ca.* 700 – 800 nm (Fig 3A), disposed usually in a chain-like structure due to the accretion effect. These diameters are in good accordance with the value extracted from FESEM studies. A deeper look into their internal structure revealed a concentric

arrangement of the graphitic planes (as demonstrated by HRTEM *vide infra*).[6] In addition, the distance between the graphitic planes also matches with that calculated from Bragg´s equation according to the XRPD spectrum (*vide supra*).

Interestingly, these chain-like structures can be disassembled by sonication, obtaining relatively stable suspensions of **CS** exhibiting the characteristic Tyndall-Faraday effect. Concretely, by suspending the powder in toluene (1 mg of **CS** in 10 mL) and submitting it to bath sonication during 30 min, almost all of the aggregates can be individualized. Fig. 3B and C depicts an HRTEM image showing the presence of isolated and monodisperse spheres, retaining their intrinsic structure. In their spherical surface, some broken edges can be seen, due to the disaggregation of the clusters after the sonication process. Furthermore, Dynamic Light Scattering (DLS) was carried out with this suspension, in order to further study the size distribution of the sample (Fig. 3D), as well as the possible presence of bigger clusters. We observed that the average hydrodynamic diameter –a complex function that describes a Gaussian distribution– is centred on *ca.* 780 nm, in good agreement with the electron microscopy observations and the classification proposed by Serp *et al.*[5]

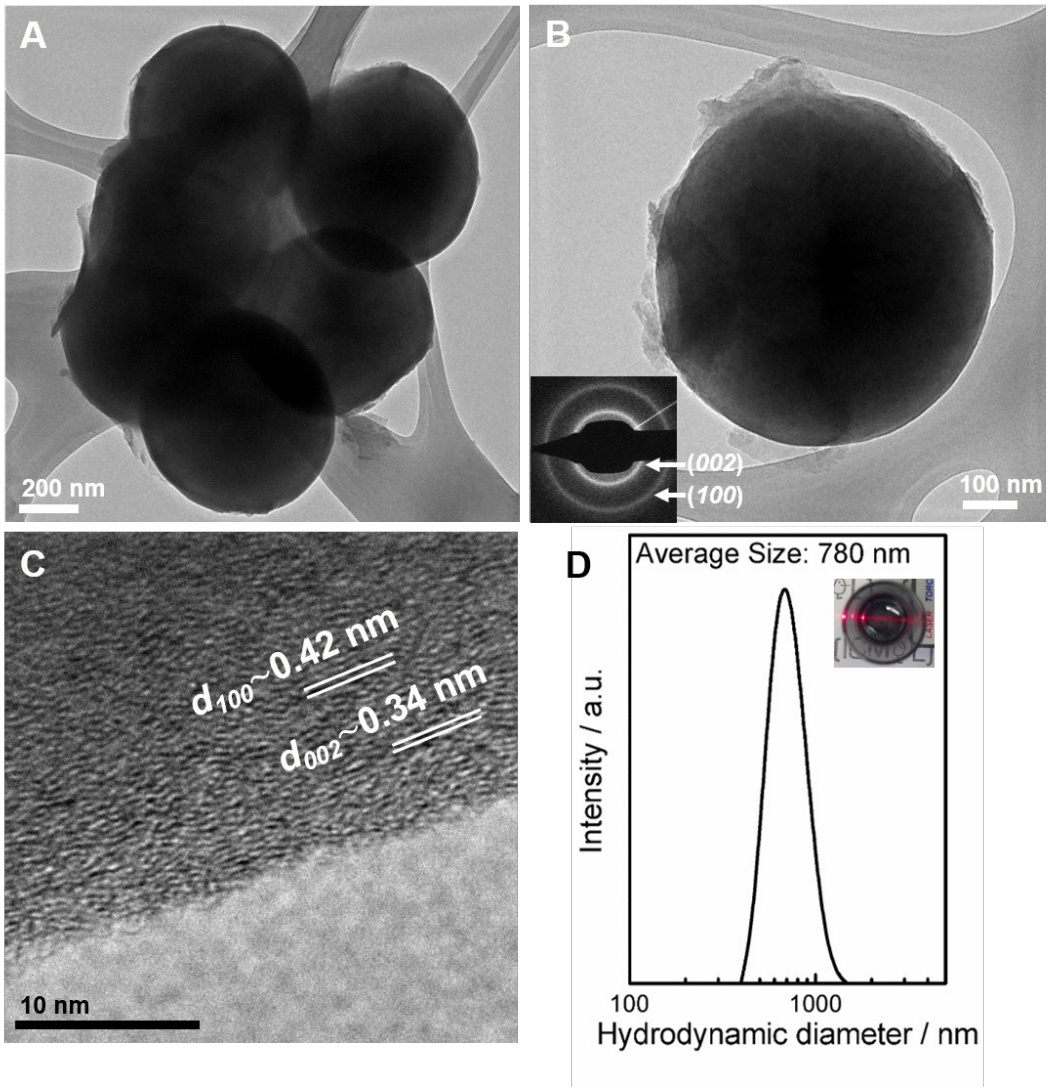

Figure 3. HRTEM image depicting (A) a cluster of spheres, disposed in a chain-like structure, and (B) a single sphere from the **CS** sample after a sonication procedure in toluene. The inset in (B) shows the selected area electron diffraction (SAED) pattern displaying two rings related with (*002*) and (*100*) planes. (C) High magnification image of the interface from a single sphere, highlighting the (*002*) and (*100*) planes and the distance between crystallographic lattices (D). Distribution of sizes extracted from DLS measurements for **CS**. Its inset shows the visible Tyndall-Faraday effect, resulting from the scattering of the irradiated beam by the particles in a toluene solution.

In order to determine the surface texture of the spheres, N_2 adsorption-desorption isotherms were measured. The **CS** showed a BET surface area value of 16.2 m^2 g^{-1}, indicative of the absence of mesoporosity on its surface, in accordance with previously published works.[10] On the contrary, carbon spheres with mesoporous structure depicted larger BET surface areas of *ca.* 1400 – 1600 m^2 g^{-1}.[36,37] It is worth to say that this value is slightly higher than that exhibited by the pristine spheres (3.6 m^2 g^{-1}), as a consequence of the annealing treatment. In line with that, differential pore volume

distribution by DFT of the spheres has been calculated, suggesting the presence of ultramicropores (See SI 8).[44]

One of the most important fields of application of **CS** and related nanomaterials is the energy storage and conversion.[45,46] Among others, supercapacitors (SCs) are attracting increasing attention due to the potential to deliver high power densities in short periods of time with high cyclability and durability.[47] In this sense, the graphitic character, porosity, conductivity or the presence of oxygen functionalities could greatly affect the properties of SCs, providing us with important information about the presence of oxygen functionalities on the surface.

For comparative purposes, we have tested the electrochemical properties of the **CS** as electrode materials for SCs in a conventional three-electrode cell. The powdered sample was mixed with acetylene black and poly-vinylidene fluoride at a mass ratio of 80:10:10 with ethanol. The mixture was cast on a 1cm^2 Ni-foam collector, dried and pressed to minimize the loss of the active material during the electrochemical testing. The electrochemical properties were measured by means of cyclic voltammetry (CV) using 6M KOH (99,99 %) as the electrolyte under an applied voltage range of 0 to -1 V (vs. Ag/AgCl). Fig. 4A shows the quasi-rectangular cyclic voltammograms recorded at different scan rates, in which the large areas suggest an appropriate supercapacitive behaviour, although these **CS** are not porous, indicative of an activated surface.[48] Moreover, galvanostatic charge–discharge cycling was also measured in order to study the specific capacitance of these **CS** (Fig. 4B). A relatively large discharge capacity of *ca*. 132 $F \cdot g^{-1}$ was obtained for a current density of 1 $A \cdot g^{-1}$ (inset in Fig. 4B), overpassing that recently reported for related microporous **CS**,[49] a clear indication of the improved graphitic quality of the as-synthesized materials and the presence of an oxidized shell in accordance with the EDAX and elemental analysis results (*vide supra*). Because the oxygen content has a close relationship with carbonization temperature, the electrochemical properties of **CS** synthesized at 1000 ^{o}C were measured, exhibiting lower values of capacitances as seen in SI 9. This fact can be related with the minor presence of oxygen on the surface of those spheres, as revealed by XPS (SI 6.1).

The potential electrochemical impedance spectroscopy (EIS) shows a Nyquist plots with a nearly vertical line, typical of capacitive behaviour. In the inset of Figure 4 can be seen a minor increase in the imaginary part due to the electrolyte resistance. The corresponding conductance shows a typical behaviour, with values close to zero at low frequencies and increased with increasing frequency, with a maximum of 1.3 S.[50]

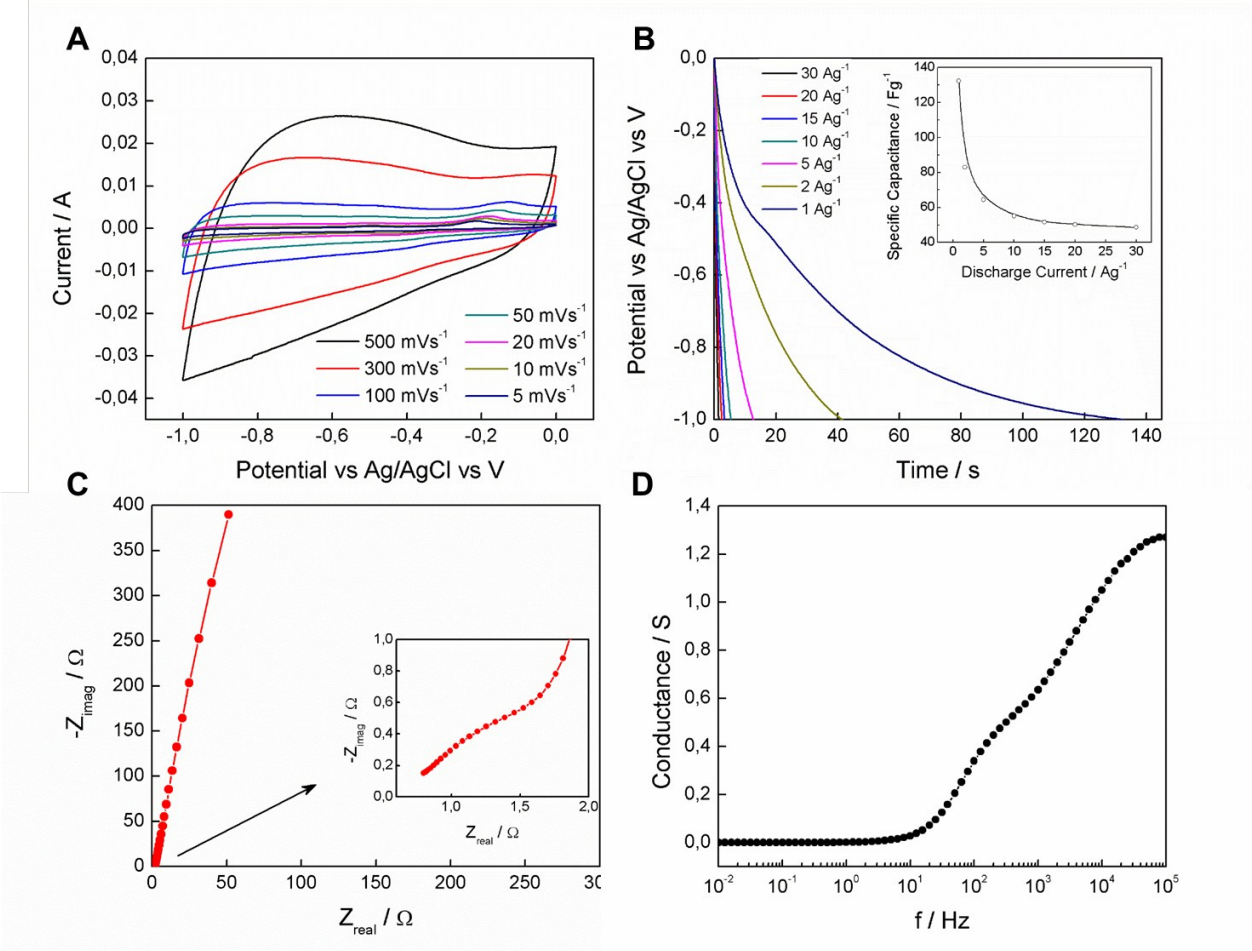

Figure 4. Electrochemical properties of **CS**. (A) CV curve at various scan rates in a 6 M KOH aqueous solution. (B) Galvanostatic discharge curves at different discharge current densities. The inset represents the specific capacitance of the material at different discharge current densities. Electrochemical impedance spectra of **CS** in a 6 M KOH electrolyte. (C) Nyquist plots and (D) the response of conductance at different frequencies.

A complete physical characterization of the **CS** has been done measuring the transport properties by four-probe method. The **CS** exhibited a nonmetallic behaviour as can be observed in the thermal evolution of the resistance (Fig. 5). Fig. 5 shows characteristic non-linear and symmetrical I-V curves for the whole studied temperature range. The non-linearity increases when the temperature is reduced, observing semiconductor behaviour. The electrical conductivity at room temperature is $1.92 \cdot 10^{-2}$ S·cm^{-1} and it is reduced four orders of magnitude when the temperature decreases, being $1.32 \cdot 10^{-6}$ S·cm^{-1} at 2 K (Fig 5). Furthermore, the conductivity matches perfectly with others values reported in the literature for **CS**.[16,17]

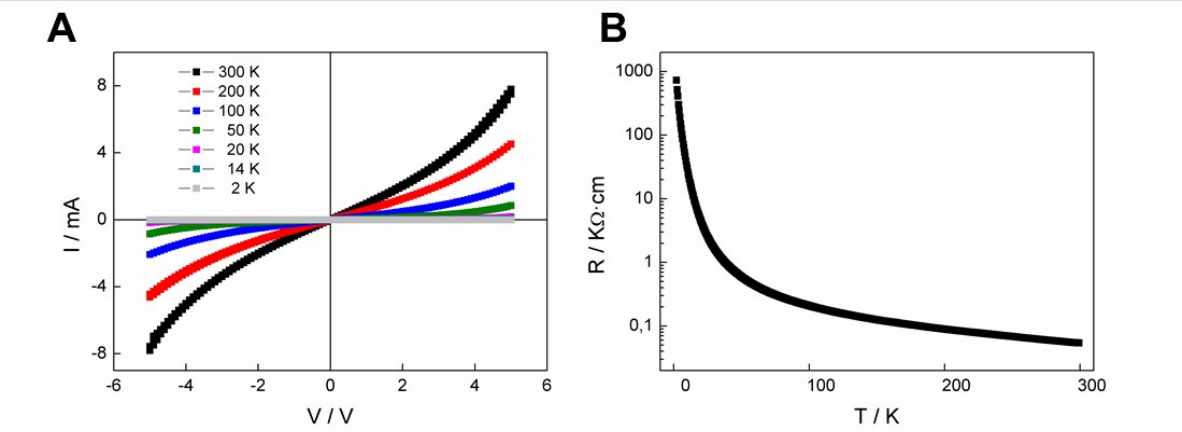

Figure 5. (A) I-V curves for a temperature range from 300 K to 2 K. The electrical conductivity at room temperature is $1.92 \cdot 10^{-2}$ $S \cdot cm^{-1}$. (B) Thermal resistance dependence of the **CS**.

Works dealing with the electrical properties of CS are very scarce. To the best of our knowledge, the first work that has measured the electrical properties of the CS is from Coville *et.al*. [16,17], where they study the electrical transport mechanisms in Nitrogen and Boron-doped carbon spheres. These works show that the dominant conduction mechanism in pristine CS is the Mott variable range hopping (Mott VRH). In our case, this model provides a good description of the thermal dependence of electrical conductivity in the 300K–2K temperature range (Fig SI 10). Thus, the experimental behaviour is well fitted by the expression $\sigma(T)=\sigma_0 \cdot \exp[-(T_0/T)^n]$, with n=1/4. The VRH model of conductivity represents a phonon-assisted mechanism of charge transport and it is normally associated with amorphous semiconductors, semiconductor glasses[51,52] and more recently with amorphous carbon.[17]

We also measured the magnetoresistance (MR) properties of **CS** under applied fields of 8 T in a PPMS system, revealing an intrinsic magnetoresistance (MR) of *ca.* 72 % at low temperatures (Fig 6). MR is calculated as $MR\ (\%) = [(R(H) - R(0)/R(0)] \cdot 100$, where R(H) is the resistivity under magnetic field B and R(0) is the resistivity without any magnetic field. As long as we increase the temperature, the MR falls dramatically until no signal is observed above 100 K.

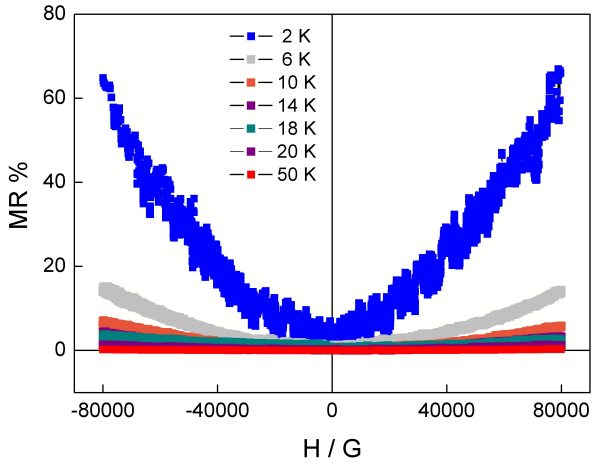

Figure 6. (A) MR dependence with the temperature of the **CS**.

Figure 6 shows a positive and non-saturated MR that decrease dramatically when temperature increases for all the temperature range studied (from 50 K to 2 K). This positive, non-saturated MR behavior has been also found for other crystalline and amorphous nanocarbons and carbon composites.[20–25] All the experimental data of the Fig 6 were fitted with the relation of MR ^ $(\mu_0 \cdot \mu \cdot |H|)^2$ (Fig. SI 10). The quadratic term is related to the ordinary MR (OMR)[20] due to the curving of electron trajectories in the carbon plane which results in a positive MR, and has a quadratic magnetic dependence of MR ^ $(\mu_0 \cdot \mu \cdot |H|)^2$, where the μ is mobility.[20–24] The magnetic measurements revealed a very small magnetic phase in the **CS** (Fig. SI 11). This magnetic phase probably comes from a small rest of the catalyst. However, XPS analysis of the **CS** showed the absence of the catalyst on the sample surface, highlighting the residual character of the catalyst present in the **CS** (Fig. SI 6.2). Therefore, the influence of the magnetic rest of the catalyst in the MR is very weak, and almost negligible.

Finally, the dramatic temperature dependence of the MR (Fig.SI 12) is an indication of the predominant contribution of the OMR to the MR observed in the **CS**. These results pave the way for using **CS** not only as a reinforcing agent of polymers, but also as electronically active building blocks in the design of hybrid multifunctional composites.

4. Conclusions

Carbon spheres with a diameter of *ca.* 740 nm have been synthesized in gram-scale proportions by means of a CVD method using NiFe-LDHs as catalyst precursor.

Control experiments revealed that the presence of the $FeNi_3$ catalyst allows us to control the size distribution, giving rise to a monodisperse sample. XRPD and Raman spectroscopy demonstrate their graphitic nature, with an I_D/I_G ratio of *ca.* 0.80, therefore exhibiting a higher degree of graphitization than other spheres reported to date. Moreover, these **CS** can be individualized in toluene by means of sonication, beating the accretion effects. Furthermore, FIB-SEM experiments show that the inner structure of the spheres is solid and consists on concentric graphitic planes. Concerning their surface properties, nitrogen adsorption, XPS and electrochemical testing revealed the presence of redox functionalities on their surface behaving as appropriated electrode materials for supercapacitors despite their intrinsic nonporous nature.

Finally, their transport properties have also been studied, exhibiting a semiconducting behaviour at low temperatures and a giant magnetoresistance of *ca*. *72* % at 2 K and a voltage of 3 V. The MR was strongly dependent on the temperature and principally has a quadratic dependence, following an ordinary MR behaviour. These **CS** are promising candidates for polymer reinforcement and as building blocks for preparing more complex hybrid composites.

Acknowledgments

Financial support from the EU (FET-OPEN 2D-INK. Grant agreement 648786), the Spanish MINECO (Project MAT2014-56143-R), the Junta de Andalucía (PAI research group TEP-946 INNANOMAT) and the Generalitat Valenciana (Prometeo and ISIC-Nano Programs) is gratefully acknowledged. Co-funding from UE is also acknowledged. TEM measurements were carried out at DME-SCCYT-UCA. We thank the Universidad de Valencia for support from VLC/CAMPUS and INNCIDE program, and for a predoctoral grant (to J.A.C.). G. A. thanks the EU for a Marie Curie Fellowship (FP7/2013-IEF-627386).

5. References

1 H. W. Kroto, J. R. Heath, S. C. O'Brien, R. F. Curl and R. E. Smalley, *Nature*, 1985, **318**, 162–163.
2 J. L. Delgado, M. Herranz and N. Martín, *J. Mater. Chem.*, 2008, **18**, 1417–1426.
3 *Ind. Eng. Chem.*, 1928, **20**, 991–993.
4 Z. C. Kang and Z. L. Wang, *J. Phys. Chem.*, 1996, **100**, 5163–5165.
5 P. Serp, R. Feurer, P. Kalck, Y. Kihn, J. L. Faria and J. L. Figueiredo, *Carbon*, 2001, **39**, 621–626.
6 M. Inagaki, *Solid State Ion.*, 1996, **86**, 833–839.
7 M. Inagaki, *Carbon*, 1997, **35**, 711–713.
8 Y. Xia, B. Gates, Y. Yin and Y. Lu, *Adv. Mater.*, 2000, **12**, 693–713.
9 A. A. Deshmukh, S. D. Mhlanga and N. J. Coville, *Mater. Sci. Eng. R Rep.*, 2010, **70**, 1–28.
10 A. Nieto-Márquez, R. Romero, A. Romero and J. L. Valverde, *J. Mater. Chem.*, 2011, **21**, 1664–1672.
11 P. Serp and J. L. Figueiredo, Eds., *Carbon materials for catalysis*, John Wiley & Sons, Hoboken, N.J, 2009.
12 N. Fleischer, M. Genut and A. Gorodnev, *Am. Ceram. Soc. Bull.*, 2006, **85**, 27–28.
13 X. He, F. Wu and M. Zheng, *Diam. Relat. Mater.*, 2007, **16**, 311–315.
14 Y. Z. Jin, Y. J. Kim, C. Gao, Y. Q. Zhu, A. Huczko, M. Endo and H. W. Kroto, *Carbon*, 2006, **44**, 724–729.
15 F. P. Hu, Z. Wang, Y. Li, C. Li, X. Zhang and P. K. Shen, *J. Power Sources*, 2008, **177**, 61–66.
16 W. P. Wright, V. D. Marsicano, J. M. Keartland, R. M. Erasmus, S. M. A. Dube and N. J. Coville, *Mater. Chem. Phys.*, 2014, **147**, 908–914.
17 K. C. Mondal, A. M. Strydom, Z. Tetana, S. D. Mhlanga, M. J. Witcomb, J. Havel, R. M. Erasmus and N. J. Coville, *Mater. Chem. Phys.*, 2009, **114**, 973–977.
18 Y. Z. Jin, C. Gao, H. W. Kroto and T. Maekawa, *Macromol. Rapid Commun.*, 2005, **26**, 1133–1139.
19 H. Ismail, P. K. Freakley and E. Sheng, *Eur. Polym. J.*, 1995, **31**, 1049–1056.
20 H. Gu, X. Zhang, H. Wei, Y. Huang, S. Wei and Z. Guo, *Chem. Soc. Rev.*, 2013, **42**, 5907 – 5943.
21 C. Bosch-Navarro, F. Busolo, E. Coronado, Y. Duan, C. Martí-Gastaldo and H. Prima-Garcia, *J. Mater. Chem. C*, 2013, **1**, 4590–4598.
22 J. Wang, X. Zhang, C. Wan, J. Vanacken and V. V. Moshchalkov, *Carbon*, 2013, **59**, 278–282.
23 Z.-M. Liao, H.-C. Wu, S. Kumar, G. S. Duesberg, Y.-B. Zhou, G. L. W. Cross, I. V. Shvets and D.-P. Yu, *Adv. Mater.*, 2012, **24**, 1862–1866.
24 Y.-B. Zhou, B.-H. Han, Z.-M. Liao, H.-C. Wu and D.-P. Yu, *Appl. Phys. Lett.*, 2011, **98**, 222502.
25 J. Zhu, Z. Luo, S. Wu, N. Haldolaarachchige, D. P. Young, S. Wei and Z. Guo, *J. Mater. Chem.*, 2012, **22**, 835–844.
26 G. Abellán, C. Martí-Gastaldo, A. Ribera and E. Coronado, *Acc. Chem. Res.*, 2015, **48**, 1601–1611.
27 G. Abellán, E. Coronado, C. Martí-Gastaldo, A. Ribera and J. F. Sánchez-Royo, *Chem. Sci.*, 2012, **3**, 1481–1485.
28 G. Abellán, J. A. Carrasco, E. Coronado, J. P. Prieto-Ruiz and H. Prima-García, *Adv. Mater. Interfaces*, 2014, **1**, 1400184.
29 G. Abellán, J. G. Martínez, T. F. Otero, A. Ribera and E. Coronado, *Electrochem. Commun.*, 2014, **39**, 15–18.

30 G. Abellán, E. Coronado, C. Martí-Gastaldo, A. Ribera and T. F. Otero, *Part. Part. Syst. Charact.*, 2013, 853–863.
31 G. Abellán, E. Coronado, C. Martí-Gastaldo, E. Pinilla-Cienfuegos and A. Ribera, *J. Mater. Chem.*, 2010, **20**, 7451–7455.
32 R. . Langford and C. Clinton, *Micron*, 2004, **35**, 607–611.
33 Y. Li, J. Chen, Q. Xu, L. He and Z. Chen, *J. Phys. Chem. C*, 2009, **113**, 10085–10089.
34 Y. Z. Jin, C. Gao, W. K. Hsu, Y. Zhu, A. Huczko, M. Bystrzejewski, M. Roe, C. Y. Lee, S. Acquah, H. Kroto and D. R. M. Walton, *Carbon*, 2005, **43**, 1944–1953.
35 V. G. Pol, M. Motiei, A. Gedanken, J. Calderon-Moreno and M. Yoshimura, *Carbon*, 2004, **42**, 111–116.
36 L. C. Yang, Y. Shi, Q. S. Gao, B. Wang, Y. P. Wu and Y. Tang, *Carbon*, 2008, **46**, 1816–1818.
37 A. Nieto-Márquez, D. Toledano, J. C. Lazo, A. Romero and J. L. Valverde, *Appl. Catal. Gen.*, 2010, **373**, 192–200.
38 H. Qian, F. Han, B. Zhang, Y. Guo, J. Yue and B. Peng, *Carbon*, 2004, **42**, 761–766.
39 M. Liu, L. Gan, W. Xiong, Z. Xu, D. Zhu and L. Chen, *J. Mater. Chem. A*, 2014, **2**, 2555–2562.
40 M. Liu, L. Gan, W. Xiong, F. Zhao, X. Fan, D. Zhu, Z. Xu, Z. Hao and L. Chen, *Energy Fuels*, 2013, **27**, 1168–1173.
41 Y. J. Kim, M. I. Kim, C. H. Yun, J. Y. Chang, C. R. Park and M. Inagaki, *J. Colloid Interface Sci.*, 2004, **274**, 555–562.
42 W. Li, D. Chen, Z. Li, Y. Shi, Y. Wan, G. Wang, Z. Jiang and D. Zhao, *Carbon*, 2007, **45**, 1757–1763.
43 D. Fujikawa, M. Uota, T. Yoshimura, G. Sakai and T. Kijima, *Chem. Lett.*, 2006, **35**, 432–433.
44 M. Liu, J. Qian, Y. Zhao, D. Zhu, L. Gan and L. Chen, *J Mater Chem A*, 2015, **3**, 11517–11526.
45 M. Liu, X. Ma, L. Gan, Z. Xu, D. Zhu and L. Chen, *J Mater Chem A*, 2014, **2**, 17107–17114.
46 D. Zhu, Y. Wang, L. Gan, M. Liu, K. Cheng, Y. Zhao, X. Deng and D. Sun, *Electrochimica Acta*, 2015, **158**, 166–174.
47 F. Beguin and E. Frackowiak, *Supercapacitors: Materials, Systems and Applications*, John Wiley & Sons, 2013.
48 X. Ma, L. Gan, M. Liu, P. K. Tripathi, Y. Zhao, Z. Xu, D. Zhu and L. Chen, *J. Mater. Chem. A*, 2014, **2**, 8407–8415.
49 W. Yang, Y. Feng, D. Xiao and H. Yuan, *Int. J. Energy Res.*, 2015, **39**, 805–811.
50 Y. Gao, Y. S. Zhou, M. Qian, X. N. He, J. Redepenning, P. Goodman, H. M. Li, L. Jiang and Y. F. Lu, *Carbon*, 2013, **51**, 52–58.
51 N. F. Mott, *Philos. Mag.*, 1969, **19**, 835–852.
52 N. F. Mott and M. Kaveh, *Adv. Phys.*, 1985, **34**, 329–401.

Table of Contents:

Text:

Herein we report the gram-scale synthesis of graphitic carbon spheres with solid inner cores, which exhibit supercapacitive properties and magnetoresistance.

ToC: